Journal of Radiation and Nuclear Applications
An International Journal

http://dx.doi.org/10.18576/jrna/100206

Theoretical Production of Copper-64 and Copper-67 and its Application in Radiotherapy

George Edusei[*]

Department of Physical & Mathematical Sciences, University of Environment & Sustainable Development, Somanya, Ghana.

Received: 02 Jan. 2025, Revised: 09 Mar. 2025, Accepted: 11 Mar. 2025.

Published online: 1 May 2025.

Abstract: The Talys-1.6 code, a nuclear reaction model, was employed to generate cross-sectional data for potential reaction paths leading to the production of copper-64 and copper-67 in a theoretical analysis. The optimal nuclear processes identified for producing ^{64}Cu/^{67}Cu involved the reactions ^{64}Ni (p, n)^{64}Cu and ^{70}Zn (p, α) ^{67}Cu. Analysis of the cross-section data for the ^{64}Ni (p, n) ^{64}Cu reaction indicated that copper-64 production is most effective within a proton energy range of 7MeV to 12MeV. Similarly, the cross-section data for the ^{70}Zn (p, α) ^{67}Cu reaction suggested that copper-67 generation is most efficient with proton energies ranging from 13MeV to 18MeV. The findings suggest that the production of ^{64}Cu/^{67}Cu is feasible in Ghana, provided low-energy cyclotrons (7MeV to 18MeV) are available, and production can be achieved with variable beam currents ranging from 50 to 200A. Comparison of different cross-sectional data with existing theoretical and experimental works in the literature showed favorable agreement. The thick target yield, determined using Simpson's numerical integration method and the radionuclide production yield equation by Qaim, resulted in thick target yields of 376MBq/A and 6.3MBq/A for the nuclear reactions ^{64}Ni (p, n)^{64}Cu and ^{70}Zn (p, α) ^{67}Cu, respectively. Additionally, this work reviews recent successful applications of copper-based radiopharmaceuticals in radiotherapy, SPECT imaging, and PET. The paper also presents intriguing findings in radioimmunotherapy, immunotherapy, and PET visualization of antibody biodistribution.

Keywords: Copper-64, Copper-67, Thick target yield, Nuclear reactions, Cross sections, Radiotherapy.

1 Introduction

The foundation of nuclear medicine lies in harnessing the radiochemical characteristics of isotopes for both treatment and diagnostic purposes in various illnesses. Approximately 45 percent of patients undergoing chemotherapy also receive radiotherapy, making it a crucial treatment avenue for addressing tumor diseases and providing palliative care for inoperable patients [3]. Theranostic pairs play a vital role in the initial imaging of radiopharmaceutical biodistribution, as radiation therapy exerts DNA-damaging, targeted, and precisely localized effects on cancer tissues [6]. Copper radioisotopes, particularly ^{60}Cu, ^{61}Cu, ^{62}Cu, and ^{64}Cu, are gaining increased attention due to their applicability in imaging, targeted radionuclide therapy (^{64}Cu and ^{67}Cu), and the provision of promising theranostic pairs, namely ^{61}Cu/^{67}Cu and ^{64}Cu/^{67}Cu.

Among these, ^{64}Cu, with its unique decay scheme involving β+ or β− decay and electron capture [27], is currently the most widely used in clinical applications. This is attributed to its therapeutic potential through beta particles (β+ or β−) and its suitability for imaging using positron emission tomography [9, 11, 16]. On the other hand, copper-67 is an attractive radioisotope for radiotherapy, boasting a sufficiently long half-life for accumulation in tumor tissue when utilized with monoclonal antibodies [13]. It undergoes complete decomposition through beta emission into the excited state of zinc isotopes.

The primary applications of copper-64 and copper-67 involve the radiolabeling of biological molecules, such as peptides and antibodies, which can be targeted towards cancers or specific cell and organ types [7]. This paper explores the theoretical production of these two copper radioisotopes, emphasizing their potential as genuine theranostic pairs. Additionally, the paper reviews recent successful applications of copper-based radiopharmaceuticals in the field of radiotherapy.

*Corresponding author e-mail: gedusei@uesd.edu.gh

2 Materials and Methods

2.1 Materials

The tools utilized in this project included a laptop, the SRIM (2013) code, and TALYS (1.6) code, which is a nuclear reaction model. TALYS is a computer code system designed for nuclear reaction analysis and prediction [17]. [29] employed SRIM, a computer software program that calculates aspects of ion transport in materials.

2.2 Method

2.2.1 Nuclear Reaction Cross Section (TALYS code)

The production of copper-67 and copper-64 involves nuclear reactions represented by the equations ^{68}Zn(p,2p)^{67}Cu, ^{70}Zn(p, α)^{67}Cu, ^{64}Ni(α,p)^{67}Cu, ^{67}Zn(n, p)^{67}Cu, ^{67}Zn(d,2p)^{67}Cu, ^{64}Ni(p, n)^{64}Cu, ^{64}Ni(d,2n)^{64}Cu, ^{nat}Ni(p , n)^{64}Cu, ^{68}Zn(p, αn)^{64}Cu, and ^{66}Zn(d, α)^{64}Cu. This process involved inputting parameters such as the incident particle, particle energy, suitable target, and the target's atomic mass into the code before submitting the data for processing. The output chamber displays aggregated cross sections of various nuclear reactions after processing. The flowchart of the TALYS software is presented below.

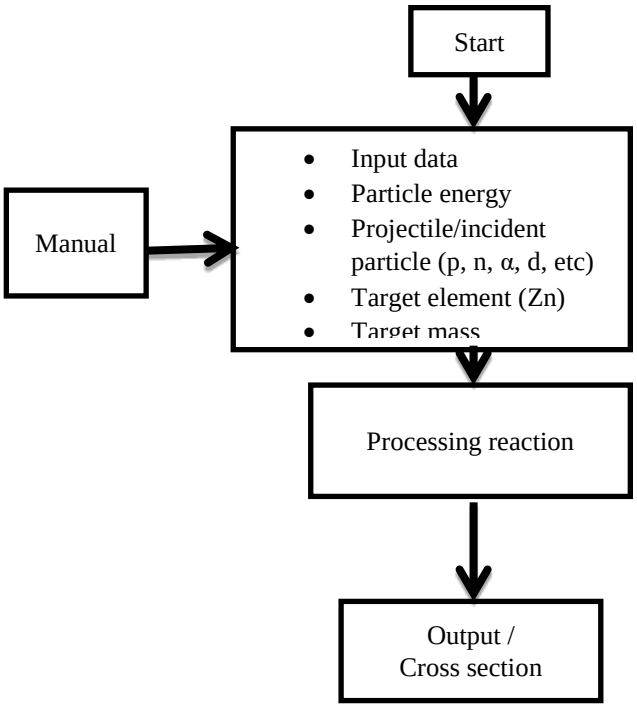

Fig. 1. Flow chart of the TALY's code [17].

The mathematical expression for cross-section is given as

$$\sigma(E) = \frac{2.678\text{x}10^{-10}\text{N}_\text{i}\text{A}}{\rho\text{tIx}} \quad (1)$$

where σ is the cross-section for a process in millibarn; A is the atomic mass of the target material in atomic mass units; N_i is the number of nuclei created during the irradiation; t is the time of irradiation in hours; ρ is the density of the target in g/cm^3; x is the thickness of the target in (μm); I is the beam current in microamperes.

2.3 Determination of Thick Target Radionuclide Production Yield

Theoretical calculations of the production yields were performed using Simpson's rule to identify a potential optimal yield in the production of ^{64}Cu and ^{67}Cu. [25] claims that the production yield(y) is provided by

$$y = \left(1 - e^{-\lambda t}\right)\frac{IN_a}{M}x\int_{E_1}^{E_2}\frac{\sigma(E)}{S(E)}dE \quad (2)$$

where

N_a is the Avogadro number, M is the target atomic weight of the target element$\sigma(E)$ is the reaction cross section as a function of energy, λ is the decay constant of the product, t is the time of irradiation, I is the projectile current and $S(E)$ is the target stopping power (SRIM, 2013) expressed in unit MeVcm^2/g [7].

Hence, the mathematical expression for the stopping power S(E) is given by

$$S(E) = \frac{144Zz^2}{AE}In\left(\frac{2195E}{Ip}\right) \quad (3)$$

Where

S(E) is the stopping power; Z is the atomic number of the target; z is the atomic number of the projectile; E is the particle energy in MeV, and Ip is the ionization potential of the target.

Equation (2) provides the thick target radionuclide production yield (y), while equation (1) provides the cross section, σ(E). By substituting equations (1) and (3) into equation (2), the equation becomes

$$y = (1 - e^{-\lambda t})\frac{IN_A}{M}x\int_{E_1}^{E_2}\times\frac{AE}{144Zz^2}In\left(\frac{2195E}{Ip}\right)dE \quad (4)$$

Where the limit E_1 and E_2 represent the incident proton energy and exit proton energy, respectively

Table 1: Some constants in a radionuclide production yield

Name of constant	Value
Avogadro's number, N_a (atoms)	6.022×10^{23}
Number of nuclei present during irradiation, Ni (atom)	9.41×10^{19}
Number of nuclei present during irradiation, Zn (atom)	8.85×10^{19}
Density of Ni, ρ (g/cm^3)	8.89
Density of Zn, ρ (g/cm^3)	7.14
Atomic number of Ni, (Z)	28.00
Atomic number of Zn, (Z)	29.00
Atomic mass Ni-64(amu) for ^{64}Cu	64.00
Atomic mass Zn-70(amu) for ^{67}Cu	70.00
Atomic number of protons, z	1.00
Target thickness of Zn, x (μm)	1400
Irradiation time for ^{67}Cu, (hrs)	3.00
Ionization energy (I_p) for Ni→64	7.6398
Ionization energy (I_p) for Zn→70	9.3942

Bringing out some constants and simplifying equation (4) becomes

$$Y = 1.86x10^{-12}(1 - e^{-\lambda t}) \, x \frac{N_A A^2 N_i}{M\rho t x Z z^2} x \int_{E_1}^{E_2} \frac{E}{In\left(\frac{2195E}{Ip}\right)} d \qquad (5)$$

If I denote that $K_1 = 1.86x10^{-12}(1 - e^{-\lambda t})$ and $K_2 = \frac{N_A A^2 N_i}{M\rho t x Z z^2}$

Then equation (5) can be written as

$$Y = K_1 K_2 x \int_{E_1}^{E_2} \frac{E}{In\left(\frac{2195E}{I\,p}\right)} dE \qquad (6)$$

By substituting some values in table (1) into equation (5), and the production yield equation becomes

$$Y = \frac{4923286.1}{tx} \int_{E_1}^{E_2} \frac{E}{In(233.65E)} dE \qquad (7)$$

Substituting the irradiation time, thickness, and particle energies for both Ni/Zn and integrating the above equation using Simpson's numerical integration with an interval of 8, the final radioisotope production yield were determined for each nuclear reaction.

3 Results and Discussion

In this investigation, an assessment was conducted on the production yield and cross-sectional data related to the synthesis of copper-64 and copper-67. Various nuclear reactions were analyzed, and trends in production yields and cross sections were graphically presented.

Examining the Cross Sections for the ^{64}Ni (p, n) ^{64}Cu Reaction [11], Figure 2 illustrates that the cross section for the mentioned reaction, leading to the generation of ^{64}Cu, initiates an increase at 10 MeV. Subsequently, it gradually declines between 13 MeV and 16 MeV before experiencing a rapid decrease at 19 MeV. The maximum cross section, recorded at 10 MeV, is 765.6 mb. Figure 2 provides a comparison between the cross section for the ^{64}Ni (p, n) ^{64}Cu reaction derived from this study (2023) using Taly's code and the cross sections obtained by [28, 26], and [1]. While the maximum cross sections from [26] and Aslam [1] show good agreement with values of 656 mb and 636 mb at the same energy, the cross sections from this study and [28] align well with the maximum values of 765.6 mb and 797 mb at 10 MeV. The cross sections from this study, [28], [1], and [26] exhibit a gradual decline as energy levels increase. However, the theoretical results from this study and [28] are slightly higher than the experimentally determined reaction cross section by [26] and [1]. Despite a shift in peak location, these cross sections continue to follow a similar pattern.

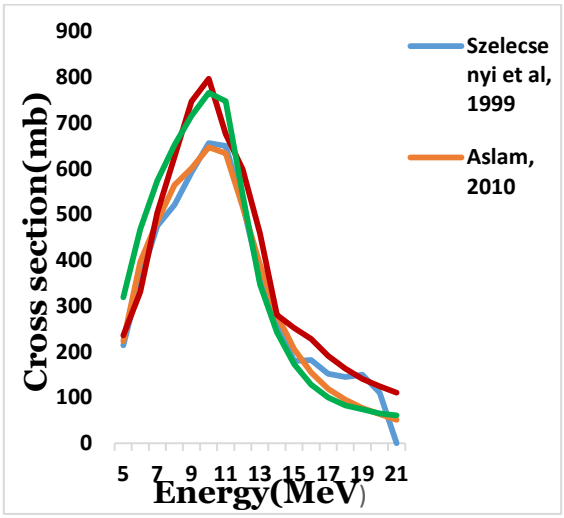

Fig.2. Cross section for ^{64}Ni (p, n) ^{64}Cu reaction.

3.1 Cross Sections for the ^{68}Zn (p, αn) ^{64}Cu Reaction.

In Figure 3, a comparison is presented between the cross section computed in this study using Taly's code (2023) for the ^{68}Zn (p, n) ^{64}Cu reaction [11] and the cross section determined by [1] based on an experimental measurement of the same reaction. It is evident that, in both studies, the cross section undergoes a significant increase from 16 MeV to 30 MeV. The maximum cross sections for both works align well, with values of (51.4 mb) at 24 MeV and (50.3 mb) at 26 MeV. Both cross sections exhibit an exponential rise from their respective peak values to approximately 27 MeV, after which they stabilize and continue to increase with energy.

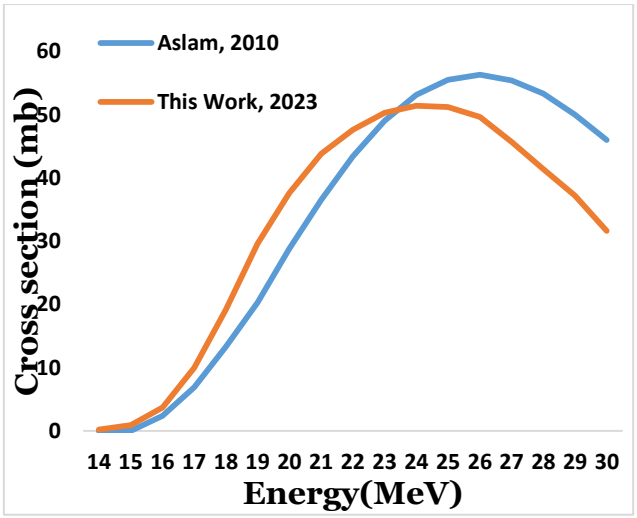

Fig. 3. Cross section for ^{68}Zn (p, αn) ^{64}Cu reaction.

3.2 Cross Sections for the ^{64}Ni (d, 2n) ^{64}Cu Reaction

In reference to the reaction ^{64}Ni (d, 2n) ^{64}Cu, responsible for the synthesis of ^{64}Cu, [11], cross-sectional data were analyzed for this study, [28], and [1], all obtained through experimental means for the same reaction. It is evident that the cross sections in all three investigations sharply increased from 6 MeV to reach their maximum values: 861 mb and 772 mb at 14 MeV, and 917 mb at 13 MeV according to [28]. While this outcome closely aligns with experimental data, discrepancies were observed in the energy range above 14 MeV. Notably, the experimentally measured reaction cross sections by [28] are slightly higher than the theoretically obtained values in this study for the same energy range, as depicted in Figure 4 below.

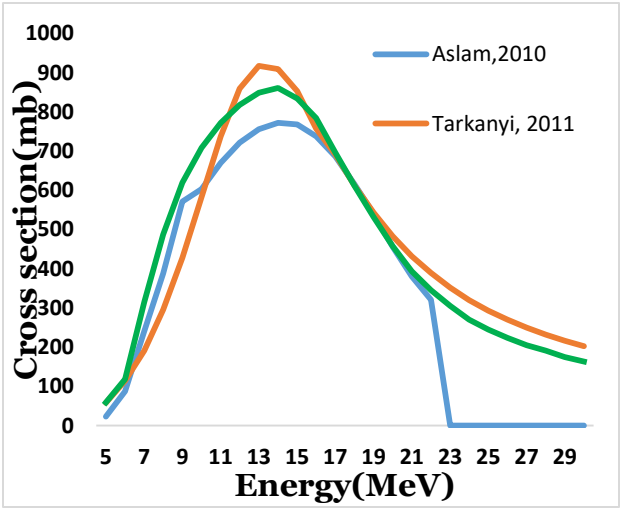

Fig. 4. Cross section for ^{64}Ni (d, 2n) ^{64}Cu reaction.

3.3 Cross Sections for the ^{70}Zn (p, n) ^{67}Cu Reaction

[14] and [28] also identified the same reaction through experimental methodologies. It has been observed that the cross sections in all three studies experienced a significant increase from 20 MeV onwards. At 50 MeV, the largest cross section in this study is 16 mb, whereas [14] and [28] recorded values of 9.9 MB and 8.2 MB, respectively. However, as illustrated in Figure 5 below, the experimentally determined reaction cross section is smaller than the theoretically calculated one in this study within the same energy range.

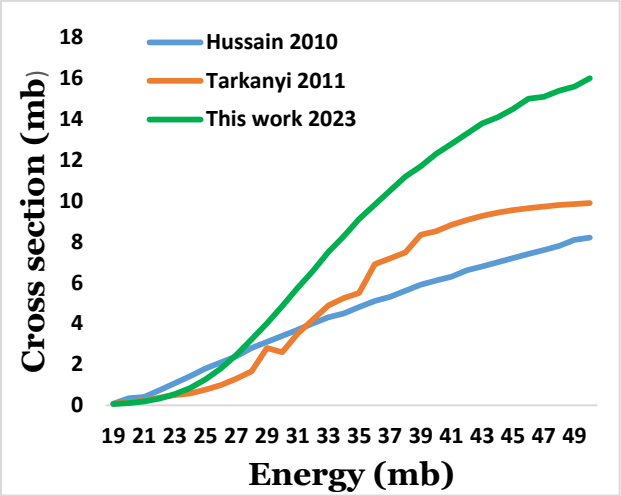

Fig. 5. Cross section for ^{70}Zn (p, α) ^{67}Cu reaction.

3.4 Cross Sections for the ^{68}Zn (p, 2p)^{67}Cu Reaction

The reaction ^{68}Zn (p, 2p)^{67}Cu, resulting in the production of ^{67}Cu, was identified through the utilization of Talys software. Concurrently, [14] and [28] employed experimental methods to identify the same reaction. The cross sections in all three studies were observed to exhibit a significant increase, commencing at 10 MeV. The largest reported cross section in this study, at 15 MeV, is 20 mb, while those reported by [14] and [28] are 11.9 mb and 12.2mb, respectively. The experimentally determined reaction cross section, as depicted in Figure 6 below, is lower than the theoretically anticipated value in this study within the same energy range.

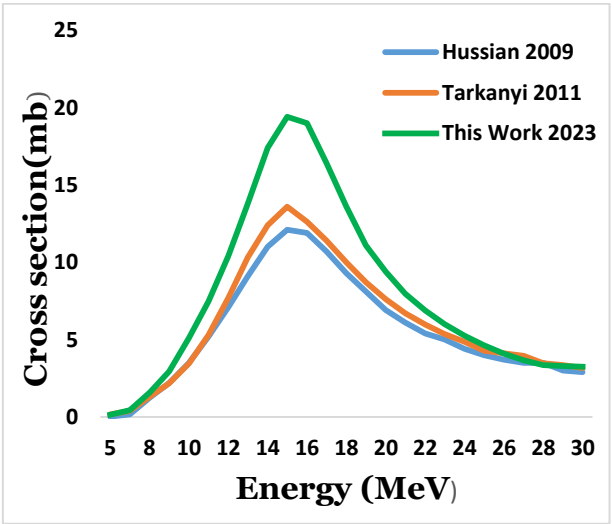

Fig. 6. Cross section for ^{68}Zn(p, 2p)^{67}Cu reaction.

3.5 Cross Sections for the ^{64}Ni (α, p)^{67}Cu Reaction

This study and the work by [14] yielded cross sections for the same reaction. Figure 7 clearly illustrates a significant increase in cross sections for both studies, spanning from 12 MeV to approximately 19 MeV. At 22 MeV, [14] graph diverges, reaching a cross section value of (22.9 mb), while this study's maximum peaks are observed at a cross section value of (19.8 mb) at 19 MeV. As both cross sections reach their zenith, they exhibit an exponential decline until around 30 MeV, after which they tend to stabilize with the rising proton energy.

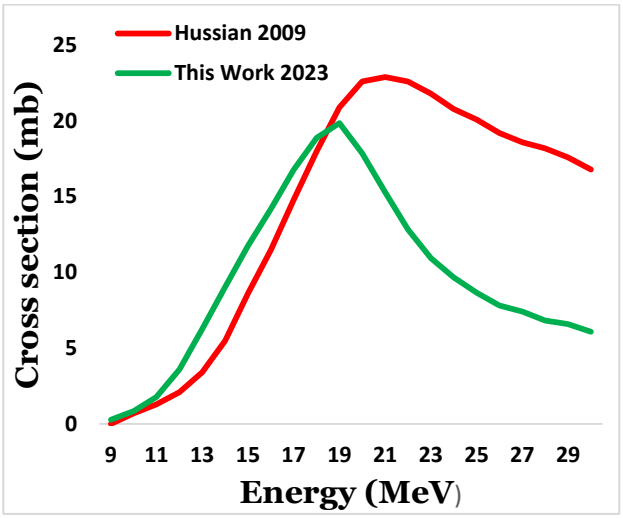

Fig. 7. Cross section for ^{64}Ni(α, p)^{67}Cu reaction.

3.6 Calculation of Yield for the Production of Copper-64 and Copper-67

Utilizing the theoretical cross-sectional data currently under discussion for the reactions: ^{68}Zn(p,2p)^{67}Cu, ^{70}Zn(p, α)^{67}Cu, ^{64}Ni(α,p)^{67}Cu, ^{64}Ni(p, n)^{64}Cu, ^{64}Ni(d,2n)^{64}Cu, and ^{68}Zn(p, αn)^{64}Cu, the production yield for Copper-64 and Copper-67 is determined. The SRIM (2013) code, which incorporates stopping power, is employed along with a specified energy range for the reactions of ^{64}Cu/^{67}Cu. These data are utilized in Equation (7) to calculate the numerical values of production yield, expressed in (MBq/μA), for each nuclear reaction and particle energy (MeV).

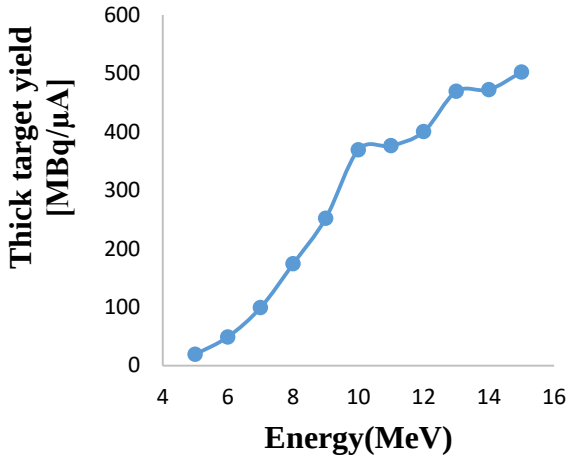

Fig. 8. Calculated thick target yield for ^{64}Ni (p, n) ^{64}Cu, reaction.

In Figure 8, it is evident that the production yield for the ^{64}Ni (p, n) ^{64}Cu reaction rises with an increase in proton energy. Four distinct research groups, namely [18], [26], [24], and [2], have documented experimental ^{64}Cu yields for these reactions. These reported values are significantly lower than their corresponding theoretical estimates.

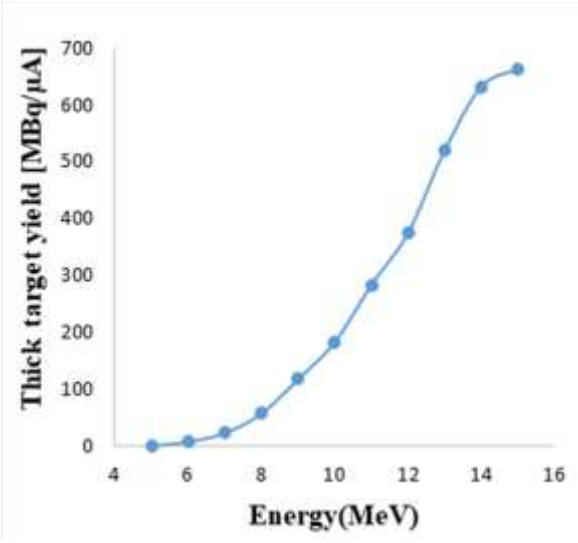

Fig. 9. Calculated thick target yield for ^{64}Ni (d, 2n) ^{64}Cu reaction.

In the context of the ^{64}Ni (d, 2n) ^{64}Cu reaction depicted in Figure 9, experimental yields were reported by [13] and [9]. Figure 10 illustrates the experimental yields for the nuclear reaction ^{68}Zn (p, αn)^{64}Cu, as reported by [3]. These reported values were notably lower than the yields calculated in the present study. The recognized reasons for the lower experimental yields include factors such as loss of activity during irradiation and chemical processing, uncertainties in high beam current measurement, radiation damage, among others. The significance of the calculated yield lies in defining the ideal (maximum) value achievable through a given reaction.

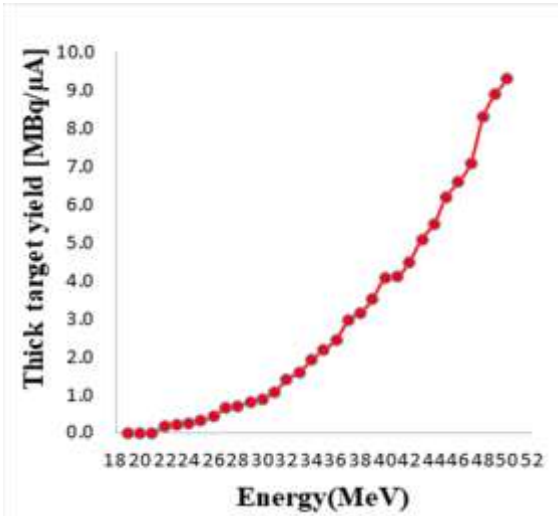

Fig. 10. Calculated thick target yield for ^{68}Zn(p, αn)^{64}Cu reaction.

Figure 11 shows the integral yield of ^{67}Cu computed for a proton-induced reaction on ^{70}Zn at 17MeV to be 6.6MBq/Ah. In contrast, Hussain (2009) reported 2.40MBq/Ah at the same energy while his works fell short of this reaction.

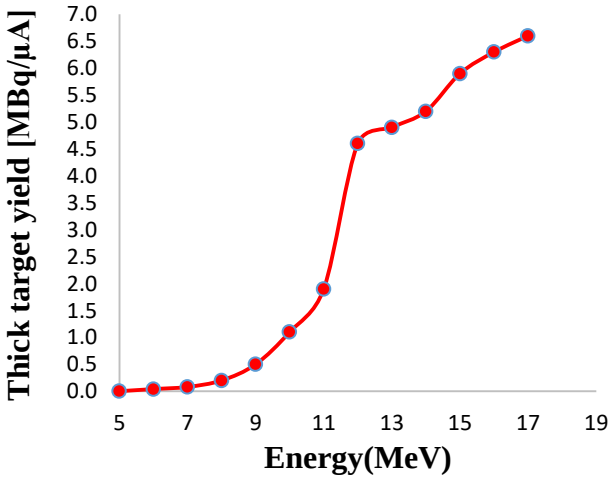

Fig. 11. Calculated thick target yield for ^{70}Zn (p, α) ^{67}Cu reaction.

Figure 12 illustrates that for protons interacting with ^{68}Zn, the anticipated yield is 2.20 MBq/Ah at 35 MeV, increasing to 4.08 MBq/Ah at 40 MeV. [14] previously determined the integral yield of ^{67}Cu as 2.0 MBq/Ah and 3.8 MBq/Ah

within the same energy range. The values obtained in this study are slightly higher than those reported by [14].

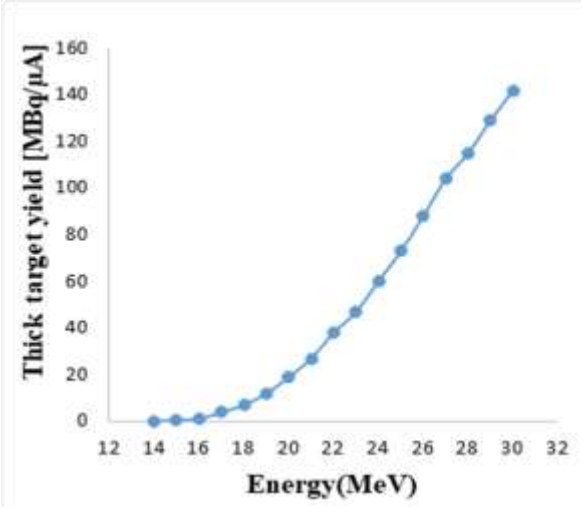

Fig.12. Calculated thick target yield for 68Zn (p, 2p)67Cu reaction.

Similar to figure 13, the predicted integral yield in this work for alpha-particles on ^{64}Ni was 26.5kBq/Ah at 15MeV and increased to 168kBq/Ah for 20MeV. Prior to [14] and [24], the yields at 15MeV and 20MeV, respectively, were calculated to be 25.3kBq/Ah and 167kBq/Ah. Their standards fell short of this work.

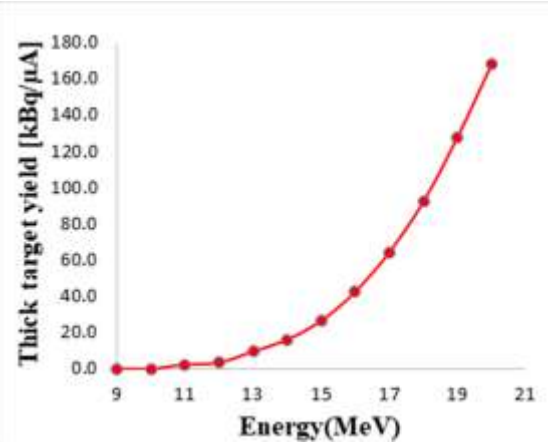

Fig.13. Calculated thick target yield for ^{64}Zn (α, p)^{67}Cu reaction.

4 Discussion

4.1 Comparison of Data of Copper-64 Production

Three of the four nuclear reactions listed in this work [^{64}Ni (p, n)^{64}Cu, ^{64}Ni(d,2n)^{64}Cu, ^{68}Zn (p, αn)^{64}Cu] were processes. Figure 2 compares the cross sections obtained in this study's for [^{64}Ni (p, n)^{64}Cu] reaction using the Talys code with that reported by [28], [1], and [26] for the same reaction at energies between 5 and 20 MeV. It can be seen that the cross section values obtained by [28] are slightly higher but they are in good agreement with this work. Despite the difference in cross section values, the trend of shape formation for all cross sections is almost the same. Therefore, it can be deduced that the optimum energy range for this reaction falls within 7-12MeV.

[28] carried out research to evaluate the ^{64}Cu production cross section of the ^{68}Zn (p, n) ^{64}Cu reaction experimentally. Figure 3 displays the cross section of both their previous research and this one. The highest cross section is observed to be 51.4mb. In addition, the graph's formation trend is nearly identical. The optimal energy range for the synthesis of ^{64}Cu is inferred to be between 20MeV and 29 MeV.

There is a dearth of experimental cross section data for ^{64}Ni(d,2n)^{64}Cu. [28] measured the cross section in a recent experiment utilizing enriched ^{64}Ni as the target and cross section values were also derived from [1]. Figure 4 compares the cross sections of their research and this theoretical study. The three-graph analysis reveals that there is data point variance, which may be caused by unstable experimental settings. Additionally, it can be shown that while the peak's divergence was observed in the energy range of 19–22 MeV, the result was still reasonably near to their work. The energy range between 10MeV and 18 MeV is ideal for the manufacture.

4.2 Comparison of Data on Copper-67 Production

Figure 5 compares the cross sections reported in this study with those by [28] and [14] for the reaction of ^{70}Zn(p, α)^{67}Cu at energies between 11MeV and 40 MeV. Although there is good agreement between the cross-section values produced by their work and this work, a peak variation was discovered in the energy range of 19–22 MeV. The pattern of shape development for the three cross sections is essentially the same, despite the modest variation in cross section values. The analysis of the cross sections shows that the 13–18MeV energy range is ideal.

The production cross section of the ^{68}Zn(p, 2p)^{67}Cu reaction for the synthesis of ^{67}Cu was measured theoretically and empirically by [14] and [28]. Figure 6 displays the cross sections of both their previous research and this one. Three works' cross sections were reported to increase significantly from 20 MeV to their maximum cross section of 16 mb. Except for a few data points, the graph's formation trend is essentially the same. The optimal energy range for the

synthesis of ^{67}Cu can be inferred to be between 45 and 50 MeV.

Additionally, [14] conducted a theoretical analysis to enhance the production of ^{67}Cu. In their research, they measured the nuclear reaction cross section for the ^{64}Ni(, p)^{67}Cu reaction, which yields ^{67}Cu for energies between 5MeV and 50 MeV. Figure 7 compares the cross sections of their research and this theoretical study. The cross sections for this work are a little lower than those of [14], and the two plots' trends and shapes are nearly identical, peaking at about 19.8 mb. Additionally, the optimal energy range for the synthesis of ^{67}Cu is 17–20 MeV as inferred from both cross sections.

4.3 Comparison of Production Routes of Copper-64

Table 2. Compares the different nuclear processes analyzed in this work with reference to the generation of ^{64}Cu [11].

Nuclear process	Optimum energy range (MeV)	Thick Target yield (MBq/μA)
^{64}Ni(p, n)^{64}Cu	12→ 7	99-369
^{64}Ni(d,2n)^{64}Cu	18→10	182-664
^{68}Zn(p, αn)^{64}Cu.	29→20	169-568

4.4 Comparison of Copper-64 Production Processes

Among the examined procedures, the technological development and current production status of the ^{64}Ni(p, n)^{64}Cu reaction stand out. This is primarily attributed to the practicality of using a low-energy proton cyclotron (Ep 7 MeV) capable of generating beam currents ranging from 50 to 150μA, which fulfills manufacturing requirements. On the contrary, the ^{64}Ni(d,2n)^{64}Cu process has not been extensively utilized for significant-scale production. Despite the substantial chemical processing involved, the ^{68}Zn(p, n)^{64}Cu reaction offers an advantage as ^{64}Cu is obtained as a byproduct during the production of ^{67}Ga. The gathered datasets are valuable for determining optimal pathways for producing ^{64}Cu using cyclotrons or accelerators, with the ^{64}Ni(p, n)^{64}Cu reaction identified as the most efficient method for producing substantial amounts of high-purity ^{64}Cu.

4.5 Comparison of Copper-67 Production Routes

Various processes, including ^{64}Ni(α, p)^{67}Cu, ^{68}Zn(p, 2p)^{67}Cu, and ^{70}Zn(p, α)^{67}Cu, can yield the medicinal radioisotope ^{67}Cu. Analysis suggests that, if low-energy cyclotrons are available, the ^{70}Zn(p, α)^{67}Cu reaction is the preferred approach due to its benefits in radiochemical purity. However, the expensive cost of enriched ^{70}Zn targets is a drawback. Alternatively, if high-energy proton beams are accessible, the ^{68}Zn(p, 2p)^{67}Cu reaction becomes more favorable, despite the challenge of separating ^{67}Cu from significant levels of ^{67}Ga produced during proton irradiation of enriched 68Zn. The ^{64}Ni(α, p)^{67}Cu procedure is considered less crucial due to its lower yield of ^{67}Cu and the high cost of the enhanced target material.

5 Copper ^{64}Cu/^{67}Cu Application in Radiotherapy

The use of "theranostic pairs" involving radiopharmaceuticals with the same molecular target tagged with imaging/therapy radionuclides is the foundation of radioligand theranostic therapy [21]. This enables sequential PET/SPECT imaging and radiation, facilitating accurate dosimetric computation [19]. The utilization of copper isotopes, specifically cyclotron-produced copper-64, has advantages over clinically used fluorine-18 and gallium-68, such as a longer half-life, allowing for extended tumor imaging [20]. Despite similar image quality with 18F-FDG, copper-64 offers improved PET image sharpness due to its lower positron energy and smaller positron mean range [15].

Copper's well-established coordination chemistry allows the use of the same chelators for both ^{64}Cu and ^{67}Cu-based radiopharmaceuticals, facilitating sequential PET imaging and radiotherapy [5, 21]. The chemical identity of imaging (^{64}Cu) and therapeutic (^{67}Cu) copper isotopes enables their use as a theranostic combination, gaining increased interest with the recent availability of high-purity and high-activity ^{67}Cu [22]. Copper-based radiopharmaceuticals, such as [^{64}Cu] [Cu (ATSM)], have demonstrated efficacy in PET imaging of tumor hypoxia, with ongoing clinical trials for rectum cancer imaging [30-32].

6 Conclusion

This study comprehensively investigated the production of Copper-64 and Copper-67, emphasizing their applications in radiotherapy. The ^{64}Ni(p, n)^{64}Cu reaction emerged as the most efficient method, with an ideal energy range of 7 to 12 MeV and a thick target production yield of 369MBq/μAh. For ^{67}Cu production, the ^{70}Zn(p, α)^{67}Cu reaction was identified as the preferred approach within the energy range of 13-18 MeV, boasting a thick target production yield of 6.50MBq/Ah.

The theranostic potential of copper isotopes, particularly the $^{64}Cu/^{67}Cu$ combination, holds promise in the treatment and diagnosis of various disorders. The successful production of ^{67}Cu in adequate quantity and purity has sparked increased interest in these applications. The efficiency and vast potential of copper-containing radiopharmaceuticals for imaging and therapeutic purposes are evident from the fruitful outcomes observed in this study.

Acknowledgment

The author expresses gratitude to the Accelerator Research Centre, Physics Department at the Ghana Atomic Energy Commission (GAEC) for their complete support of this research. The financial support for this research has been provided by individuals.

References

[1] M. N. Aslam, S. Sudár, M. Hussain, A. A. Malik, and S. M. Qaim, Charged particle induced reaction cross section data for production of the emerging medically important positron emitter 64Cu, Radiochim. Acta., **97**, 669–686, 2010.

[2] M. Avila-Rodriguez, C. Rios, J. Carrasco-Hernandez, J. Manrique-Arias, R. F.O Martinez-Hernandez,. A. Jalilian, E. Martinez-Rodriguez, M. Romero-Piña, and A. Diaz-Ruiz, Biodistribution and radiation dosimetry of [64Cu] copper dichloride: First-in-human study in healthy volunteers. EJNMMI Res., **7(1)**, 98–104, 2017. http://dx.doi.org/10.1186/s13550-017-0346-4

[3] T. E. Boothe, E. Tavano, J. Munoz, and S. Carroll, Coproduction of 64Cu and 67Cu with 67Ga using protons on 68Zn. J. Labelled Compd. Radiopharm., **30**, 108, 1991.

[4] R. Baskar, J. Dai, N. Wenlong, R. Yeo, K. and W. Yeoh, Biological response of cancer cells to radiation treatment. Front. Mol. Biosci., **1(24)**, 2014.

[5] A. Braune, L. Oehme, R. Freudenberg, F. Hofheinz, J. Van den Hoff, J. Kotzerke, S. Hoberück, Comparison of image quality and spatial resolution between 18F, 68Ga, and 64Cu phantom measurements using a digital Biograph Vision PET/CT. EJNMMI Phys., **9**, 1–5, 2022.

[6] E. Capasso, S. Durzu, S. Piras, S. Zandieh, P. Knoll, A. Haug, M. Hacker, C. Meleddu, and S. Mirzaei, Role of 64CuCl2 PET/CT in staging of prostate cancer. Ann. Nucl. Med., **29(6)**, 482–488, 2015. http://dx.doi.org/10.1007/s12149-015-0968-4.

[7] A. Celler, X. Hou, F. Bernard, T. and Ruth, Theoretical modelling of yield for proton-induced reaction of natural and enriched molybdenum target. Phy Med. Biol., **56**, 54-69, 2011.

[8] R. Chakravarty, P. Shetty, K. Nair, A. Rajeswari, K. Jagadeesan, H. Sarma, V. Rangarajan, R. Krishnatry, and S, Chakraborty, Reactor produced [64Cu] CuCl2 as a PET radiopharmaceutical for cancer imaging: From radiochemistry laboratory to nuclear medicine clinic. Ann. Nucl. Med., **34**, 899–910, 2020. http://dx.doi.org/10.1007/s12149-020-01522-2

[9] Daraban, L., Adam, R., and A. Hermanne, Study of the excitation function for the deuteron induced reaction on 64Ni (d, 2n) for the production of the medical radioisotope 64Cu. Journal of Applied Radiation and Isotopes., **67**,506, 2009.

[10] G. Dellepiane, P. Casolaro, C. Favaretto, P.V. Grundler, L. Mateu, P. Scampoli, Z. Talip, N.P. Van der Meulen, and S. Braccini, Cross section measurement of terbium radioisotopes for an optimized 155Tb production with an 18 MeV medical PET cyclotron. Appl. Radiat. Isot., **184**, 110-175, 2022a. http://dx.doi.org/10.1016/j.apradiso.2022.110175.

[11] G. Edusei, A. B. Andam, J. J. Fletcher, G. K. Banini, J.B. Tandoh, J. B. Simulation of Cross Section for the Production of Copper-64. Advances in Physics theories and Application., **67**, 24-29, 2017.

[12] C. Favaretto, Z. Talip, F. Borgna, P.V. Grundler, G. Dellepiane, A. Sommerhalder, H. Zhang, R. Schibli, S. Braccini, C. Müller, N. P. Van der Meulen, Cyclotron production and radiochemical purification of terbium-155 for SPECT imaging. EJNMMI Radiopharm. Chem., **6**, 37, 2021. http://dx.doi.org/10.1186/s41181-021-00153

[13] Hermanne, A., Tarkanyi, F., Takacs, S., Kovalev, G. and Ignatyuk, F. (2007). Activation Cross Sections of the 64Ni (d, 2n) Reaction for the Production of the Medical Radionuclide 64Cu, Nucl. Instr. Meth. In Physics B, 258.

[14] M. Hussain, Comprehensive evaluations of charged particle data for production of the therapeutic radionuclides 103Pd, 186Re and 67Cu. J. Kor. Phys. Soc. **59**, 1– 4, 2009.

[15] M. Jauregui-Osoro, S. Robertis, P. Halsted, S. Gould, Z. Yu, R. Paul, P. Marsden, A. Gee, A. Fenwick, and P. Blower, Production of copper-64 using a hospital cyclotron: Targetry, purification and quality analysis. Nucl.Med.Commun.,**42(9)**,1024–1038,2021. http://dx.doi.org/10.1097/MNM.0000000000001422

[16] A. Koning, .and D. Rochman, Modern Nuclear Data Evaluation with the TALYS Code System. Nucl. Data Sheets.,**113**,2841–2934,2012. http://dx.doi.org/10.1016/j.nds.2012.11.002.

[17] T. Liu, M. Karlsen, A.M Karlberg, and K.R Redalen, (2020). Hypoxia imaging and theranostic potential of [64Cu] [Cu (ATSM)] and ionic Cu (II) salts: A review of current evidence and discussion of the retention mechanisms. EJNMMI Res., **10**, 33, 2020.

[18] D. W. McCarthy, R. E. Shefer, Klinkowstein, L.A Bass, W.H. Margeneau, C.S Cutler, C. J. Anderson, and M. J. Welch, Efficient production of high specific activity 64Cu using a biomedical cyclotron. Nucl. Med.Biol.,**24(1)**,35–43,1997 http://dx.doi.org/10.1016/S0969-8051(96)00157-6.

[19] M.J. Merrick, D. A. Rotsch, A. Tiwari, J. Nolen, T. Brossard, J. Song, T. J. Wadas, J.J Sunderland, and S. A. Graves, Imaging and dosimetric characteristics of 67Cu. Phys. Med. Bio., **66**, 035002, 2021.

[20] M.J. Merrick, D. A. Rotsch, A. Tiwari, J. Nolen, T. Brossard, J. Song, T. J. Wadas, J.J Sunderland, and S. A. Graves, Half-life of 67Cu. J. Phys. Commun., **5**, 085007. 2021.

[21] C. Miller, J. Rousseau, C. F. Ramogida, A. Celler, A. Rahmim, and C. F. Uribe, Implications of physics, chemistry and biology for dosimetry calculations using theranostic pairs. Theranostics., **12**, 232–259, 2022.

[22] V.M. Miranda, Medicinal Inorganic Chemistry: An updated review on the status of metallodrugs and prominent metallodrug candidates. Rev. Inorg. Chem., **42**, 29–52, 2022.

[23] J. Nickoloff, N. Sharma, L. Taylor, Biological consequences of radiation-induced DNA damage: Relevance to radiotherapy. Genes.,**11(99)**, 2013

[24] A. Obata, S. Kasamatsu, and D.W. McCarthy, Production of therapeutic quantities of 64Cu using a 12 MeV cyclotron. Nuclear Medicine and Biology., **30(5)**, 535–539, 2003

[25] S. M. Qaim, Nuclear data for production of new medical radionuclides; J. Nucl. Sci. Technol. Suppl., **2**, 1272-1277, 2008.

[26] F. Szelecsényi, G. Blessing, and S. Qaim, Excitation functions of proton induced nuclear reactions on enriched 61Ni and 64Ni: Possibility of production of no carrier-added 61Cu and 64Cu at a small cyclotron. Appl.Radiat.Isot.,**44(3)**,575–580,1993. http://dx.doi.org/10.1016/0969-8043(93)90172-7.

[27] P. Szymański, T. Frączek, M. Markowicz, and E. Mikiciuk-Olasik, "Development of copper-based drugs, radiopharmaceuticals and medical materials," Biometals., **25**, 1089–1112, 2012.

[28] F. Tarkanyi, S. M. Qaim and R. Capote, Nuclear data for the production of therapeutic radionuclides. International Atomic Energy Agency, 2011.

[29] J. F. Ziegler, and J. M. Manoyan, The stopping of ions in compounds. Nucl. Instrum., **35**, 215, 2013. URL http://www.srim.org.

[30] Y. Zhou, J. Li, X. Xu, M. Zhao, B. Zhang, S. Deng, Y. Wu, 64Cu-based radiopharmaceuticals in molecular imaging. Technol. Cancer Res. Treat., 18, 2019.

[31] A. Wöher,., A, Ostowski., Kratz, K.-L ., Dillman, I., El-Taher, A., Fedoseyev,V., Fraile, L., Fynbo, L., Köster, U., Pfieffer, B., Ravn, I., Seliverstov, M., Shergur, J., Weissman, L., Walters W. B. and the ISOLDE Collaboration. First Gamma- Spectroscopic study of the r-process Waiting point Nucleus ^{130} Cd. Proceedings XI Workshop on Nuclear Astrophysics, Ringberg Castle at Lake Tegemsee, 11-16 February 2002, Max plank Institüt für Astrophysik, MPA/ P13, Ps 79-83. 2002.

[32] Kratz, K.-L., Dillmann,I., Arndt, O., Hannawald, M., Pfeiffer, B., Ostrowski, A, . El-Taher, A, . Wöhr, A., Shergur, J., Walters, W.B., Köster, U., Fedoseyev, V.N., Ravn, H.L, Seweryniak, D., Hoff, P., Brown, A. and the ISOLDE-Collaboration Decay of the r-process waiting-point nuclide 130Cd to levels of 130In. 2002 Fall Meeting Division of Nuclear Physics, American Physical Society; 9-12 October 2002, East Lansing, MI